An automated light yield measurement setup for liquid scintillator

Hechong Han[1,a,b], Jiaxuan Ye[a,c*], Gaosong Li[a], Liangjian Wen[a]

[a]Institute of High Energy Physics, Chinese Academy of Sciences, 19B Yuquan Road, Beijing, China.
[b]School of Physical Sciences, University of Chinese Academy of Sciences, 19A Yuquan Road, Beijing, China.
[c]China Center of Advanced Science and Technology, Beijing 100190, China.

*Corresponding author(s). E-mail(s): yejx@ihep.ac.cn;

Abstract

Tellurium-130 is a promising candidate for neutrinoless double beta decay ($0\nu\beta\beta$) search due to its high natural abundance. However, it is challenging to dope tellurium into liquid scintillator at desired level while minimumly affecting the optical properties like light yield and transparency. Lots of R&D work are needed to develop the optimized recipes, where quick and robust characterizations of samples are highly demanded. In this paper, we present an automated setup designed for the efficient and precise measurement of light yield in liquid scintillators. This setup can measure up to eight sets of samples in a measurement round. The systematic uncertainty is less than 2%. This setup is playing a crucial role in the optimization of liquid scintillator formulations.

Keywords: neutrinoless double beta decay, liquid scintillator, light yield

1 Introduction

The concept of neutrinoless double beta decay ($0\nu\beta\beta$) was proposed by W.H. Fury in 1939 [1]. The Schechter-Valle black box theorem [2] indicates that if $0\nu\beta\beta$ occurs, neutrinos must be Majorana particles, meaning that neutrino is its own antiparticle [3]. This implies a violation of lepton number conservation during the decay process, suggesting a breakdown of symmetry and the potential existence of new physics. Neutrinoless double beta decay has been a focal point in neutrino physics research, providing insights into the absolute mass scale of neutrinos.

Numerous collaborations have explored this phenomenon, including KamLAND-Zen [4],CUORE [5],PandaX [6],EXO [7], LEGEND [8] and many other experimental groups.

Tellurium (Te) is one of the prime candidates for neutrinoless double beta decay studies. Moreover, liquid scintillators are widely used in neutrino detection due to their advantageous properties. A natural extension is to incorporate tellurium into the liquid scintillator to facilitate measurements of neutrinoless double beta decay. However, it is expected that during the process of doping the scintillator with tellurium, the light yield can be significantly impacted, resulting in degraded energy resolution. Therefore, extensive measurements of light output in tellurium-doped liquid scintillator (TeLS) are necessary to optimize the formulation.

In this paper, we present the experimental design and apparatus, simulations and data analysis methods, measurement results of liquid scintillator, and error analysis.

2 Experimental design

To attain enhanced sensitivity, it is essential to maximize the tellurium doped into the liquid scintillator. However, an increasing amount of tellurium may significantly degrade the optical properties of the scintillator. Therefore, the challenge is to maintain good optical properties while doping more Te into the liquid scintillator. In our previous work [9], the 0.5% mass fraction doped TeLS has a light yield of ∼60% compared to undoped LS, with a 5% measurement error. To facilitate the optimization of the light yield, we require an automated setup capable to measure multiple samples at one time as well as suppress the measurement uncertainties.

In order to achieve the aforementioned physical objectives, we have designed an experimental apparatus. This experimental device is composed of a glove box, a rotating motor, a photomultiplier tube (PMT), and a digitizer, as shown in Figure. 1 in detail. The glove box provides an anoxic environment, while the rotating motor facilitates automated batch measurements. PMT and the digitizer are utilized to receive and store the signals.

2.1 Radioactive source

The radioactive source is ^{207}Bi, with a half-life of 31.22 years [10]. The decay mode is β^+/EC, resulting in the excited decay daughter nucleus ^{207}Pb. Following the de-excitation of ^{207}Pb, internal conversion electrons are emitted with the dominant energies of 481 keV, 975 keV and 1047 keV.

The radioactive source consists of multiple discs with a diameter of 25.4 mm. These discs are compressed together by an embedded ring, with the front disc serving as a protective layer that provides isolation, while the bottom disc is coated with ^{207}Bi, functioning as the signal disc, which has an effective area diameter of 5.08 mm. The overall structure of the radioactive source is compatible with the diameters of the sample bottle, PMT, and support structure, where the diameter of the effective component is significantly smaller than that of the sample bottle. Consequently, minor positional variations of the radioactive source discs within the support structure will not result in substantial changes in the deposition of the effective component within the sample.

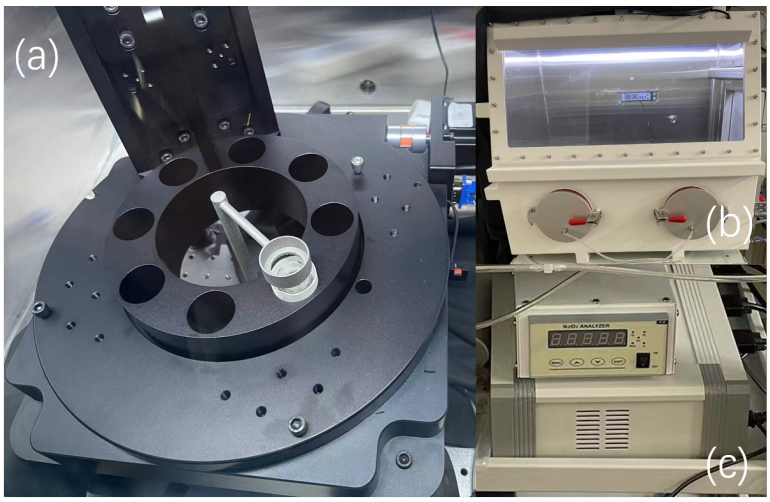

Fig. 1: (a) The rotating motor with eight sample holders. The radioactive source is positioned on the grey support frame directly above the sample bottle, while the PMT is located on the support frame directly below it. (b) The glove box. (c) The oxygen monitor (up) and the motor controller (down).

2.2 Glove box

Oxygen molecules in liquid scintillator can cause quenching effect, reducing the light yield [11]. Therefore, we require a glove box to maintain the entire experimental setup in an oxygen-free environment through a vacuuming and nitrogen purging process. The glove box is the VGB-3A model whose vacuum degree is −0.1MPa from Changshu Tongrun Electronic Technology Co., Ltd. During the experiment, the glove box will not be opened to maintain a nitrogen environment. Different batches of samples on the motor are changed through the gloves of the glove box.

2.3 Rotating motor

In order to reduce systematic errors caused by different samples, a rotating motor equipped with eight identical sample holders evenly distributed in angle is designed. It is adapted from Y200RA300 model from Beijing Jiangyun Optoelectronic Technology Co., Ltd. The diameter of each sample holder is 26 mm, slightly larger than that of the sample bottle (25 mm). A reflective film made of Tyvek is added to enhance the collection efficiency of scintillation light. The rotating motor can be remotely controlled by a computer and can be programmed to move in a custom way. During the measurement, the radioactive source and PMT remain stationary, and the sample to be tested is moved to the position by the rotating motor.

The accuracy of the motor rotation is crucial in ensuring that each rotation places the sample in the same position consistently. The step size of the rotation motor is one degree. We tested the repeatability of the rotation and find the impact to light collection efficiency is expected to be negligible. After eight rotations of 45 degree, the sample reaches exactly the same position. Any rotation

accuracy introduced uncertainty are evaluated and properly included as part of the position dependent uncertainty in Sec. 5.

2.4 PMT

The PMT used is R1924A from Hamamatsu. It is about 25 mm in diameter which couples to the size of the sample bottle. The most sensitive wavelength is 420 nm to match the peak wavelength of the liquid scintillation [12]. The PMT is operated at a high voltage of 1100 V, with a gain of 7.5×10^6.

2.5 Digitizer

The PMT signal is digitized and readout by the NDA6110 model digitizer from Jinan Laboratory of Applied Nuclear Science. It is a 4-channel, 14-bit, 1 GSPS device. The pulse width of the signals in this experiment is on the order of tens of nanoseconds. Waveforms are saved for offline analysis.

2.6 Measurement procedure

The first step of the experiment involves vacuuming the glove box. The sample bottle placed inside the glove box is opened in advance. As the vacuuming process progresses, the gas pressure difference between the inside and outside of the sample increases, causing the oxygen in the sample to be continuously released to the exterior and pumped away by the vacuum pump. Once the pressure in the box reaches the limit of the vacuum pump, the vacuum pump is stopped and the air extraction valve is closed, maintaining the glove box at ultra-low pressure for one day. During this period, the oxygen content in the sample continues to decrease. Subsequently, nitrogen with a purity of 99.9999% is introduced into the box to restore it to normal pressure. The experiment is not conducted in a vacuum environment to prevent the insulation performance of the PMT base from deteriorating, which could lead to discharge and damage. The oxygen level in the glove box is kept at approximately 300 ppm.

The measurement of the first sample is conducted after properly configuring the parameters of the PMT and the digitizer. Once a sufficient amount of data has been accumulated, the digitizer will stop taking data. At this point, the motor will rotate the next sample to the measurement position. Subsequently, the digitizer will resume recording the data. This process will continue until all samples have been measured. By properly programming the start and end time of the motion of the motor and the data taking of the digitizer, a fully automated measurement process can be achieved. This ensures precise and efficient data collection.

3 Simulation

A Geant4 simulation is built to guide the design and help understand the expected spectrum from the ^{207}Bi in the setup. A simplified geometry is used as shown in Figure 3. The liquid scintillator (LS) has the same composition of JUNO LS [12] which utilizes LAB as the solvent, mixed with 2.5g/L PPO as fluor and 3mg/L bis-MSB as wavelength shifter. The simulation restored the experimental setup for light yield measurement, including key elements such as:

- Precise positioning and dimensions of the radioactive source, sample bottle, and PMT.
- Incorporation of Tyvek reflective film surrounding the sample bottle and the

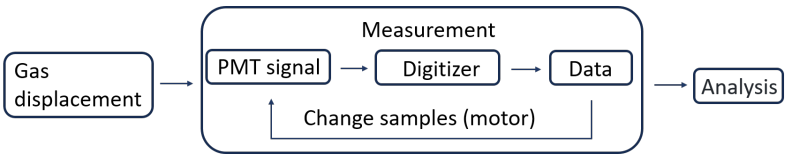

Fig. 2: Measurement procedure of light yield measurement. Detailed information is described in the main text.

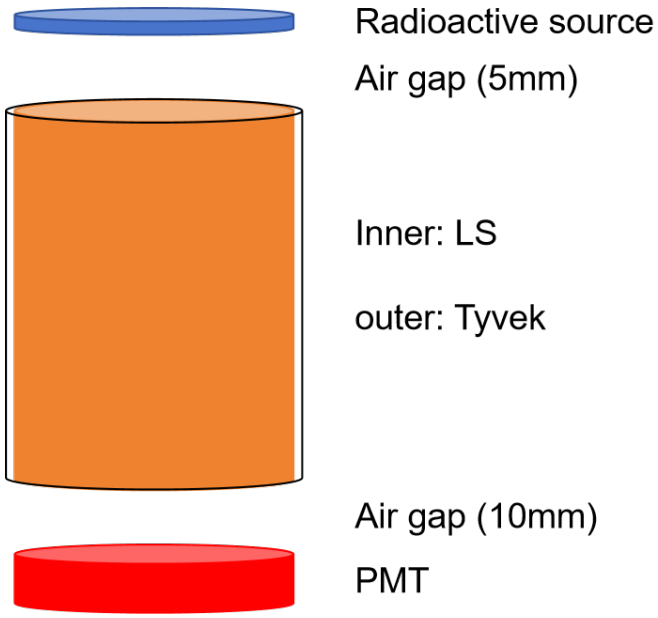

Fig. 3: Simplified geometry in Geant4 simulation.

air gap between the sample and the radioactive source.

- Inclusion of various physical processes like scintillation and Cherenkov process, Rayleigh scattering, refraction, and attenuation.

Following the simulation of one million events, the distribution of ^{207}Bi deposited energy is depicted in Figure 4. The energy deposition histogram reveals two distinct sets of adjacent main energy peaks along with their corresponding Compton platforms. The first set includes electrons with energies of 481 keV and 553 keV, while the second consists of electrons with energies of 975 keV and 1047 keV. Notably, peaks with higher energy exhibit less disturbance and higher resolution, making them ideal for energy calibration.

4 Data measurement and analysis

In the experiment, we arranged eight liquid scintillator samples. Each sample is measured for 15 minutes to accumulate at least 50000 events. Maintaining a

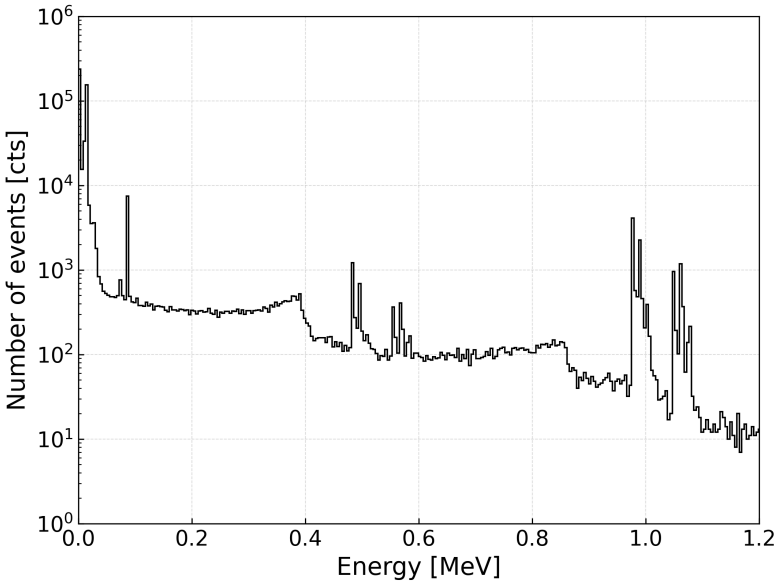

Fig. 4: Energy deposition in liquid scintillator.

consistent environment during each measurement round, including factors such as temperature, humidity, and the operational status of the PMT, helps minimize systematic errors.

4.1 Waveform analysis

The waveform has 1000 sample points at 1 ns sampling interval. The triggering condition for the signal is that there are 8 consecutive points that show a monotonically increasing trend (rising edge), with all exceeding the set threshold of 4 mV. The trigger point is set at position 100, allowing for the calculation of the baseline using data prior to the trigger point, specifically by averaging the values from the 10th to the 80th points. By examining the waveform data, as shown in Figure 5, the signal duration is estimated to be approximately 60 nanoseconds. In this analysis, the integral charge is calculated using the integral of the difference between the values from the 90th to the 160th points and the previously obtained baseline.

The measured data spectrum is compared with the MC simulation as shown in Figure 7. The main peak in the data spectrum is dominated by the contribution from conversion electrons around 1 MeV. Data and MC simulation shape agree reasonably well at high energy end. This peak is used to characterize the light yield for different samples.

4.2 Spectrum fitting

The charge spectrum for the ^{207}Bi source is fitted to determine the peak position. In actual data analysis, the limited resolution can significantly affect the energy distribution, causing the main energy peak to deviate from a simple Gaussian representation. To be compared with a simple Gaussian function fitting, we expanded the fitting range to include the Compton plateau preceding

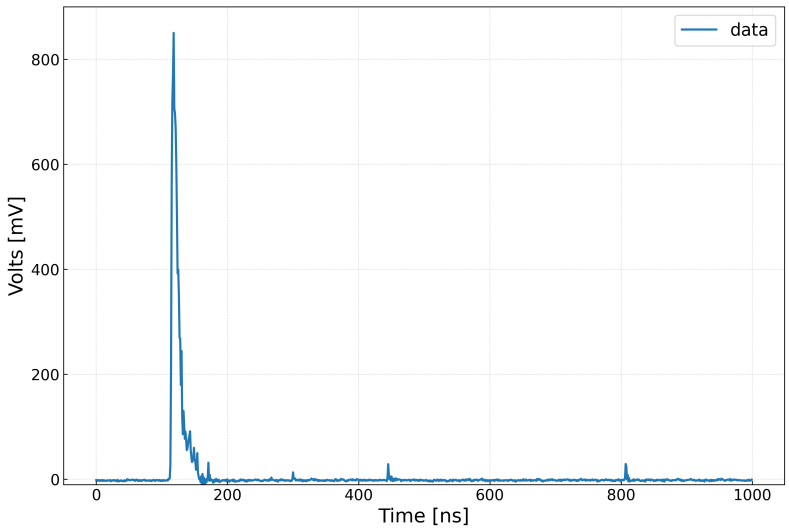

Fig. 5: Waveform of light yield measurement for LS.

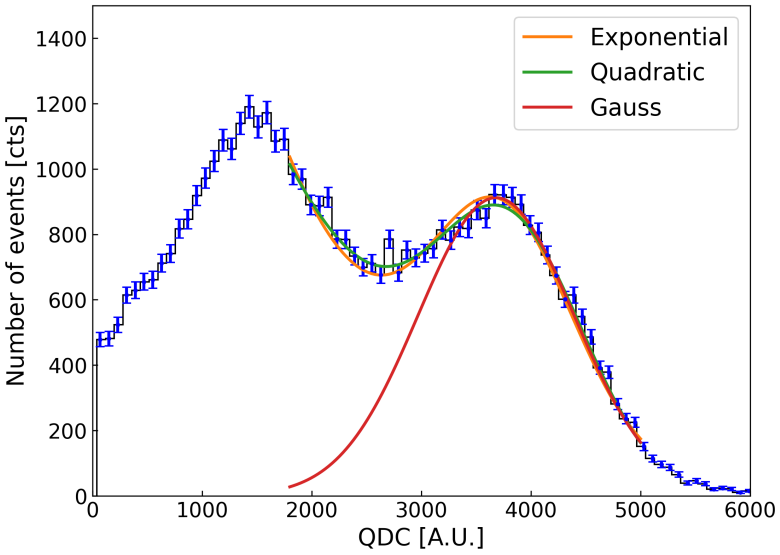

Fig. 6: Measurement and fitting results for a LS sample.

the peak position and employed a combination of quadratic, exponential, and Gaussian functions for the fitting process in Figure 6. Among these three results, the quadratic function and the Gaussian function yielded the smallest χ^2 value which is very close to that of a simple Gaussian function. Nevertheless, The variations in peak values, which will be used for the calculation of relative

light yield, obtained from different fitting methods will be discussed in section 5. In order not to include additional systematic error, we used a simple Gaussian fitting for all samples.

5 Systematic error

As previously noted, variations in sample positioning can introduce systematic errors in individual measurement rounds, while changes in the experimental environment between different rounds can also contribute to these errors. Additionally, small discrepancies in sample content during preparation, variations in the manufacturing process of the sample bottles, as well as the fitting method described in section 4 can further introduce systematic errors.

To quantify these systematic errors, we use non-doped standard liquid scintillator for study. We distribute the standard liquid scintillator equally among eight sample bottles for measurement, ensuring that inherent differences between the samples and the bottles are considered. Following this, we conducted several rounds of measurements, in order to account for environmental variations that may arise over time.

The final measurement results are analyzed using the same fitting method applied in 4, leading to the results presented in Figure 8.

- **Position** A difference in measured light yield for the same samples placed in different sample holders are observed. The difference is at 6% level at most as shown in Figure 8. This difference is repeatable and is expected to be mostly caused by the fitness of Tyvek in the holder. We take one measurement as the nominal correction for the position dependent difference. Different measurements at different times showed the deviation at different positions after correction is mostly within 2%. We take the RMS from those values and assigned 1.9% position dependent uncertainty.
- **Environmental conditions** By analyzing the variations in light yield of samples at the same position across different measurement in Figure 8, the systematic errors introduced by measurements from different cycles can be identified. The data indicate that the systematic error associated with position is significantly greater than that caused by variations in environmental conditions. This is largely due to the effective temperature control provided by the air conditioning, which minimizes temperature fluctuations in $\pm 0.5°C$. Additionally, the sealed environment of the glove box ensures that changes in oxygen content during a single measurement round do not significantly impact the results.
- **Fitting method** By analyzing the effects of different analytical methods applied to the same sample, the systematic errors introduced by the various analytical approaches can be identified as shown in Figure 6. This includes differences in the fitting functions for a single fitting of the same sample, as well as variations in the fitting ranges due to minor discrepancies in spectral shapes observed across multiple measurements.

In summary, through statistical analysis of the data, the final value of the systematic error can be obtained as shown in Table 1.

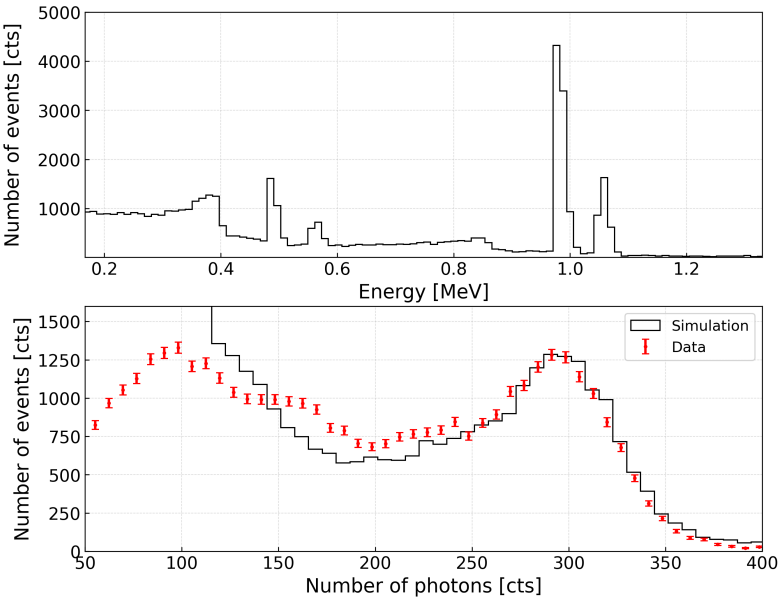

Fig. 7: Energy deposition revisited and total photons received in PMT in simulation.

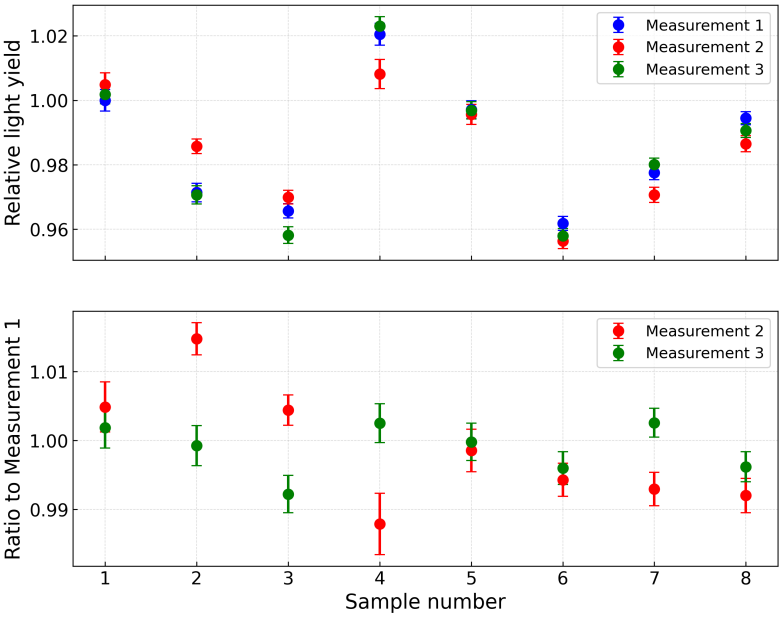

Fig. 8: Light yield for Standard LS in different locations and measurements.

	Systematic errors
Location	1.9%
Environmental conditions	0.4%
Fitting method	0.3%
Total	2.0%

Table 1: Results for systematic errors.

6 Conclusion

In this study, we developed an automated measurement system to accurately determine the light yield of LS. This system allows for simultaneous measurement of up to eight Te-LS samples. The results demonstrated that the system could achieve a systematic error of approximately 2.0%, meeting the stringent requirements for optimizing Te-LS formulations. This automated system not only enhances the efficiency of batch testing but also provides a robust framework for future research on Te-LS. By enabling precise light yield measurements, this innovation paves the way for optimizing the composition of Te-LS, thereby improving their performance in detecting rare events like neutrinoless double beta decay.

Acknowledgements

This work was supported in part by the National Natural Science Foundation of China under Grants No. 12141504 and No. 12125506, and by the State Key Laboratory of Particle Detection and Electronics, China under Grant No. SKLPDE-KF-202201.

References

[1] Furry, W.H.: On transition probabilities in double beta-disintegration. Phys. Rev. **56**, 1184–1193 (1939) https://doi.org/10.1103/PhysRev.56.1184

[2] Schechter, J., Valle, J.W.F.: Neutrinoless double beta decay in SU(2) × U(1) theories. Phys. Rev. D **25**, 2951–2954 (1982) https://doi.org/10.1103/PhysRevD.25.2951

[3] Avignone, F.T., Elliott, S.R., Engel, J.: Double beta decay, majorana neutrinos, and neutrino mass. Rev. Mod. Phys. **80**, 481–516 (2008) https://doi.org/10.1103/RevModPhys.80.481

[4] Collaboration, K.-Z.: Search for the majorana nature of neutrinos in the inverted mass ordering region with kamland-zen. arXiv preprint **arXiv:2203.02139** (2022) https://doi.org/10.48550/arXiv.2203.02139

[5] Collaboration, C.: Search for majorana neutrinos exploiting millikelvin cryogenics with cuore. Nature **604**, 53–58 (2022) https://doi.org/10.1038/s41586-022-04497-4

[6] Collaboration, P.: Searching for neutrino-less double beta decay of xe-136 with pandax-ii liquid xenon detector. Chinese Physics C **43**(11), 113001 (2020) https://doi.org/10.1088/1674-1137/43/11/113001

[7] EXO Collaboration: The exo-200 detector for the enriched xenon observatory. Physics Procedia **31**, 123–135 (2012)

[8] LEGEND Collaboration: The legend experiment: Neutrinoless double beta decay search with germanium detectors. Physical Review C **104**(4), 045502 (2021)

[9] Ding, Y.-Y., Liu, M.-C., Wen, L.-J., Li, Y.-x., Li, G.-s., Zhang, Z.-y.: A novel approach in synthesizing te-diol compounds for tellurium-loaded liquid scintillator. Nuclear Instruments and Methods in Physics Research Section A: Accelerators, Spectrometers, Detectors and Associated Equipment **1049**, 168111 (2023) https://doi.org/10.1016/j.nima.2023.168111

[10] Kondev, F.G., Lalkovski, S.: Nuclear Data Sheets for A = 207. Nucl. Data Sheets **112**, 707–853 (2011) https://doi.org/10.1016/j.nds.2011.02.002

[11] Hua-Lin, X.: Oxygen quenching in LAB based liquid scintillator and nitrogen bubbling. Chin. Phys. C **34**, 571–575 (2010) https://doi.org/10.1088/1674-1137/34/5/011 arXiv:0904.1329 [nucl-ex]

[12] Abusleme, A., *et al.*: Optimization of the JUNO liquid scintillator composition using a Daya Bay antineutrino detector. Nucl. Instrum. Meth. A **988**, 164823 (2021) https://doi.org/10.1016/j.nima.2020.164823 arXiv:2007.00314 [physics.ins-det]